ISBN: 978-3-95450-214-1 ISSN: 2673-5490 doi:10.18429/JACoW-IPAC2021-WEPAB367

BUBBLE GENERATION IN THE SNS 2 MW MERCURY TARGET

C. Barbier†, J. Weinmeister, F. Rasheed, K. Johns,
D. Winder, B. Riemer, D. Ottinger, M. Costa, R. Sangrey
Oak Ridge National Laboratory, Oak Ridge, TN, USA

Abstract

A 2MW prototypical target was built and tested at the Target Test Facility, a mercury process loop available at Oak Ridge National Laboratory. Acrylic viewports on the top of the target were used to determine the bubble size distribution (BSD) generated by the swirl bubblers. It was found that the bubblers were not only capable of generating small bubbles (i.e. less than 150 μm diameters) but that the BSD was independent of gas injection rate.

INTRODUCTION

The accelerator at the Spallation Neutron Source (SNS) is currently being upgraded to increase the proton beam power from 1.4 MW to 2.8 MW. About 2 MW will go to the [1] first target station, while the rest will go to the future second target station. The first target station uses a stainless steel vessel in which mercury flows. When it is hit by the short proton beam pulse, strong pressure waves are developed inside the mercury and the vessel itself causing weld failures and cavitation damages. The pressure wave can be significantly mitigated by injecting small helium bubbles into the mercury [1-3]. The SNS has been injecting helium bubbles in the target since 2017 using small orifices but has met challenges with orifices clogging during fabrication and operation, which lowers the gas injection rate below design values. Since gas injection will be critical for operation at 2 MW, a new gas injection method was developed. The Japan Proton Accelerator Research Complex (J-PARC) mercury target uses swirl bubblers [4] to generate small bubbles in mercury. Instead of relying on small orifices to generate small bubbles, turbulence developed from high shear flows is used to break larger gas bubbles into the desired small size. This bubbler type will be implemented at SNS in the 2 MW target and should remediate the current clogging issues causing low gas injection rates.

Due to the opacity of mercury, measuring the bubble size distribution (BSD) in mercury is challenging. The present paper describes a prototypical target fabricated with acrylic viewports to measure the bubble size. A detailed description of the bubblers is provided, and the BSDs generated are illustrated and discussed.

EXPERIMENTAL SETUP

The design of the 2MW target is based on the jet-flow design [5] with several improvements (see Fig. 1). First, the center baffle was retracted towards the back of the target: since it was on the path of the beam, it was getting too hot, and high thermal stresses were observed.

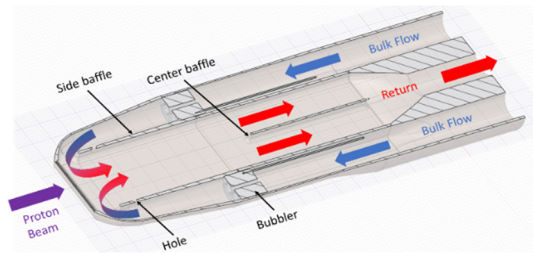

Figure 1: Horizontal cross-section view of the 2 MW target with its key features. The blue and red arrows represent the mercury flow.

To compensate for the removal of the center baffle, the front target is tapered to make it structurally stiffer at the beam entrance. Additionally, some holes were added to the side baffle to avoid forming a recirculation zone at the end of the side baffle that leads to improper cooling and higher thermal stresses on the side baffles. Also, the bubbler's location is closer to the nose to limit bubble coalescences when traveling from the bubbler to the nose. Finally, an additional gas injection site was added at the target nose, where the flow was lacking bubbles due to the flow pattern. Figure 1 shows the main flow pattern in the target: mercury flows from the main two bulk inlets towards the nose where it combines and flow toward the return. Unfortunately, this flow pattern leads to a stagnation region at the beam entrance where a lot of energy is deposited into the stainless-steel vessel and the mercury. To ensure proper cooling of the nose, an additional quasi-2D channel flow is wrapped around the nose and is referred to as the window flow (Fig. 2). The target wall facing the bulk mercury at the beam entrance has shown to be severally damaged by cavitation erosion during operation [3]. However, prior experiments suggested that the presence of flow mitigates cavitation damage [6]. Thus, an additional flow was implemented at the bottom of the target to disturb the stagnation region and is referred in this paper as the "jet-flow" (Fig. 2). This jet flow does not contain bubblers, which combined with the bulk flow stagnation region, creates the non-helium bearing region in the mercury. The additional gas injection is located just at the end of the diving board of the jet flow and allows to inject bubbles just at the beam entrance in this region. The total flow rate in the target is 214 kg/s: 89 kg/s on each bulk inlet, 23 kg/s in the jet-flow channels, and 13 kg/s in the window flow channels.

† barbiercn@ornl.gov

ISBN: 978-3-95450-214-1 ISSN: 2673-5490 doi:10.18429/JACoW-IPAC2021-WEPAB367

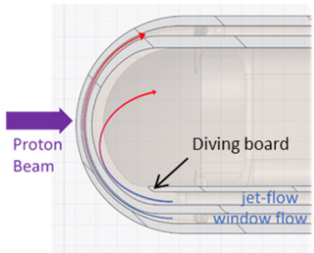

Figure 2: Vertical cross-section view of the 2 MW target at the symmetry plane.

The bubbler consists of four swirl-bubbler units that generate four vortex flows that alternatively swirl clockwise and counter-clockwise (see Fig. 3, left). This flow pattern avoids the formation of a large swirl that would enhance bubble coalescence. At the center of the bubbler, an unobstructed hole is present to decrease the pressure drop and to delay the merging of the four swirls. Gas is injected downstream of the vanes at the center of the swirl units and forms a vortex gas line until it exits the venturi, shears into small bubbles, and bends towards the wall due to the Coanda effect. The key parameters are shown in Fig. 3. The order of the bubble diameter D_b generated by the bubbler can be estimated with [7] $D_b = 1.26(\sigma/\rho)^{3/5}\epsilon^{-2/5}$, where σ is the surface tension, ρ the fluid density, and ϵ is the visco-dissipation ratio that can be estimated with: $\epsilon = D_e^2 f_e^3 = 4V_e^2\, tan^2\,\theta_f\, /D_e$ where f_e is the swirl frequency at the bubbler exit and V_e the averaged velocity in the venturi part of the bubbler (D_e). With the parameters given in Fig. 3, it was found $D_b = 72$ µm. Simulations of a simple 1D geometry suggests that bubbles with a diameter less than 100 μm are most efficient at mitigating the pressure wave [8].

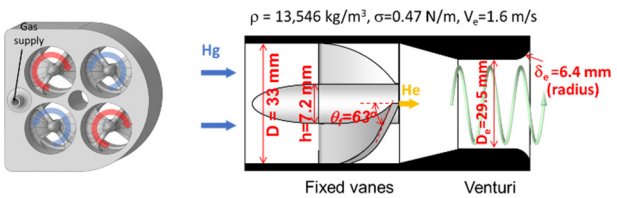

Figure 3: (left) 3D view of the swirl bubblers and the vanes orientations. (right) 2D view of a single swirl bubbler and key parameters.

A prototypical target was built and installed at the Target Test Facility (TTF) at ORNL. The TTF is a full-scale prototype of the SNS target station with a similar centrifugal pump and piping. However, the TTF does not have a large heat exchanger like SNS since the only energy that needs to be removed is generated by the friction of flowing mercury. The TTF target is similar to the 2 MW design, except there is no window flow. The window flow would prevent visualizing the bubbles, and it is not needed since there is no proton beam energy source. All the experiments were performed with a flow rate of 105 GPM in each bulk inlet and 22.5 GPM for the jet-flow. For the bubblers, a total gas injection rate ranging from 2.5 to 10 SLPM was used and was evenly distributed between the two bubblers. To measure the bubble sizes, the target is equipped with 4 acrylic ports on the top of the target return(see Fig. 4, left). In addition. The target nose is made of acrylic with flat outside surfaces to limit the optical distortion.

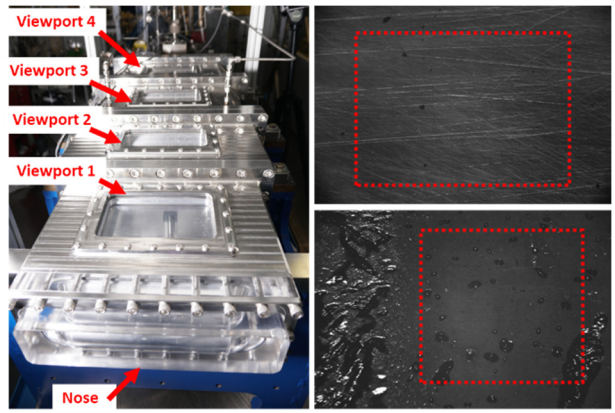

Figure 4: (left) Picture of the prototypical 2 MW target installed at TTF with the locations of the different ports. (right) Example of pictures capture at the viewport 1 (top) and 4 (bottom). The red rectangle shows the region of interest chosen for the image analysis. The width of the picture is 26.3 mm. Note the large gas pockets in viewport 4 due to bubble coalescence.

A camera is suspended above the target, and motorized linear stages are used to adjust the height and the angle of the camera. Dampers are mounted on the camera holders to ensure the camera does not vibrate excessively during measurements. A 20 MP FLIR BlackFly camera with a 0.5 x 120 mm telecentric lens with in-line illumination from Edmund optics was used to take pictures. The resolution achieved with the camera and lens combination is 4.8 µm/px. For each camera position, 300 pictures were taken. The post-processing was performed with Fiji [9]. Scratches on the acrylic ports were removed by subtracting the median picture of the stack from the images. Then the images were made binary, and the particle analyzer tool was used to measure the bubbles on the port. Bubbles that were not circular enough or were touching the edge of the Region Of Interest (ROI) were discarded. Since the small bubbles observed on the viewports have the shape of a cap of a sphere, the actual bubble diameter d_b is estimated with $d_b = 0.62\, d_{obs}$ where d_{obs} is the diameter obtained from the image analysis, and 0.62 is the correction required assuming a contact angle of 130° on the viewport [10].

RESULTS AND DISCUSSION

Very small bubbles are observed on the nose and on viewports 1 and 2. In Viewport 3, larger bubbles are observed resulting from coalescence as buoyant forces

ISBN: 978-3-95450-214-1 ISSN: 2673-5490 doi:10.18429/JACoW-IPAC2021-WEPAB367

have lifted most bubbles to the upper surface. In Viewport 4, large gas pockets are observed (Fig. 4, right). Since we are focusing on the bubble size measurements, the camera was positioned slightly away from the symmetry plane, at about one-third of the target width, and approximately at the center of the viewporton the beam direction. For viewport 4, the Region of Interest (ROI) was chosen to avoid the large gas pocket in the center of the target (Fig. 4, right). Similarly, measurements at the nose were performed at one-third of its width and in the middle of its height.

BSDs measured at the viewports and on the nose are shown in Fig. 5. As expected by the theory presented earlier, the BSD was found to be independent of the gas injection rate: very similar BSDs are observed for each port for the four gas injection rates. From viewport 1 to 4, the most probable diameter range is 50 to 75 μm and is close to what was predicted by the theory, 72 μm. From viewport 1 to viewport 4, the tail of the BSD is getting fatter, indicating the coalescence of the bubbles that leads to larger bubbles. Regardless, the BSD on Viewport 1 to 4 is similar in shape, with most bubbles with a diameter less than 150 μm (>70%). The BSD at the nose is quite different from the other viewports and follows Gaussian probability profile. Although the most probable bubble is slightly bigger (75-100 μm), all the bubbles are smaller than 275 μm. This is very encouraging as it suggests that the flow is populated with only small bubbles at the nose where the proton beam enters, before the bubbles rise and coalesce in the return channel.

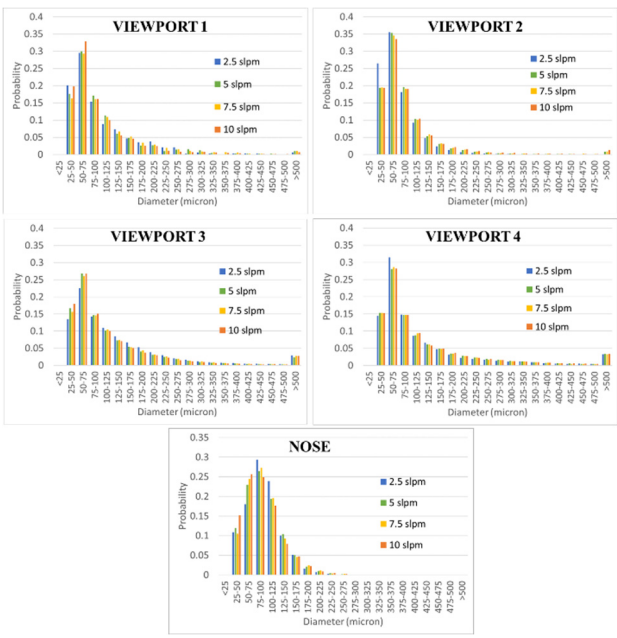

Figure 5: Bubble Size distribution observed at the different viewports.

Some measurements were also performed with 10% lower mercury flow rate. Results are not shown here, but it was found that the BSD was not strongly affected by it: the critical diameter predicted by the theory increased from 72 μm to 81 μm, but this increase could not really be observed in the BSD due to the bin sizes.

There are several uncertainties in the bubble size determination, and they are discussed in detail now. Since the bubbles are sliding on the viewport, the contact angle is not constant. A contact angle of 120° and 140° leads to a correction factor of 0.66 and 0.57, respectively. Next, the spherical cap shape assumption of the the bubbles on the viewport is not correct for larger bubbles (mm size) that are probably flatter, and thus their diameters are overestimated. Finally, the camera's resolution, 4.8 μm/px leads to an error of ± 3 μm on the true bubble diameter. Assuming the bubble shape error is negligible for small bubbles (diameter less than 150 μm), the compound error in diameter measurements are estimated to be ± 8.5%. Measurements could be improved by improving the polishing on some of the viewports (or use glass viewports instead of acrylic) and using a deep learning algorithm to detect the bubble like in previous work [11].

CONCLUSION

Measurements of helium bubbles generated by swirl bubblers in mercury were performed at the TTF on a prototypical 2 MW target using viewports on the top and nose of the target. At the front of the target where the proton beam enters, most bubbles have a diameter less than 150 μm diameter and should be effective at mitigating the pressure wave generated by the SNS proton beam. The first target with swirl bubblers is planned for operation in 2022 and will validate the efficiency of the swirl bubblers in mitigating the pressure wave.

ACKNOWLEDGMENT

This manuscript has been authored by UT-Battelle, LLC, under Contract No. DE-AC0500OR22725 with the U.S. Department of Energy. This research was supported by the DOE Office of Science, Basic Energy Science, and Scientific User Facilities. The United States Government retains and the publisher, by accepting the article for publication, acknowledges that the United States Government retains a non-exclusive, paid-up, irrevocable, world-wide license to publish or reproduce the published form of this manuscript, or allow others to do so, for the United States Government purposes. The Department of Energy will provide public access to these results of federally sponsored research in accordance with the DOE Public Access Plan (http://energy.gov/downloads/doe-public-access-plan).

ISBN: 978-3-95450-214-1 ISSN: 2673-5490 doi:10.18429/JACoW-IPAC2021-WEPAB367

REFERENCES

[1] B. W. Riemer *et al.*, "Small gas bubble experiment for mitigation of cavitation damage and pressure waves in short-pulse mercury spallation targets", *J. Nucl. Mater.,* vol. 450, no. 1-3, pp. 192-203, Jul. 2014. doi:10.1016/j.jnucmat.2013.10.011

[2] Y. Liu *et al.*, "Strain measurement in the recent SNS mercury target with gas injection", *J. Phys. Conf. Ser.,* vol. 1067, p. 052022, Sep. 2018. doi:10.1088/1742-6596/1067/5/052022

[3] D. Mcclintock *et al.*, "Laser Line Scan Characterization of Cavitation-Induced Erosion to SNS Mercury Target Vessels", ORNL, Oak Ridge, USA, Rep. ORNL/TM-2019/1103, Jan. 2019.

[4] H. Kogawa *et al.*, "Development of microbubble generator for suppression of pressure waves in mercury target of spallation source", *J. Nucl. Sci. Technol.,* vol. 52, no. 12, pp. 1461-1469, Dec. 2015. doi:10.1080/00223131.2015.1009188

[5] C. Barbier *et al.*, "Numerical and Experimental Investigation of the Flow in the SNS Jet Flow Target", in *Proc. ASME IMECE 2015,* Houston, USA, Nov. 2015. doi:10.1115/IMECE2015-51910

[6] B. W. Riemer *et al.*, "Status of R&D on mitigating the effects of pressure waves for the Spallation Neutron Source mercury target", *J. Nucl. Mater.,* vol. 431, no. 1-3, p. 160, Dec. 2012. doi:10.1016/j.jnucmat.2011.11.018

[7] C. Martinez-Bazan *et al.*, "On the breakup of an air bubble injected into a fully developed turbulent flow. Part 1. Breakup frequency", *J. Fluid. Mech.,* vol. 401, pp. 157-182, Dec. 1999. doi:10.1017/S0022112099006680

[8] K. Okita *et al.*, "Propagation of pressure waves, caused by a thermal shock, in liquid metals containing gas bubbles", in *Proc. ASME FEDSM 2005,* Houston, USA, Jun. 2005. doi:10.1115/FEDSM2005-77397

[9] J. Schindelin *et al.*, "Fiji: an open-source platform for biological-image analysis", *Nat. Methods,* vol. 9, no. 7, pp. 676-682, Jul. 2012. doi:10.1038/Nmeth.2019

[10] A. H. Ellison *et al.*, "Contact Angles of Mercury on Various Surfaces and Effect of Temperature", *J. Chem. Eng. Data,* vol. 12, no. 4, pp. 607-609, Oct. 1967. doi:10.1021/je60035a037

[11] F. Rasheed *et al.*, "Deep Learning for Intelligent Bubble Size Detection in the Spallation Neutron Source Visual Target", in *Proc. ASME IMECE 2020,* Virtual, Online, Nov. 2020. doi:10.1115/IMECE2020-23164